# Deciphering the resistance mechanism of tomato plants against whitefly-mediated *Tomato curly stunt virus* infection through UHPLC-MS based metabolomics approaches.

L Rossouw, NE Madala, F Tugizimana, PA Steenkamp, LL Esterhuizen*, IA Dubery*

Department of Biochemistry, University of Johannesburg, Auckland Park, 2006, South Africa

## Supplementary Information file S2:

## UHPLC-MS chromatograms and MS/MS fragmentation spectra of signatory biomarker metabolites identified through multivariate data analysis

### 2.1    UHPLC-HD-ESI-MS chromatograms of methanol extracts from tomato leaf tissue

*Figure S2.1 A and B: Overlay of representative original chromatograms obtained by UHPLC-HD-ESI-MS of aqueous methanol extracts from tomato leaf tissue of Control (green), whitefly treated (yellow) and viruliferous whitefly treated (red) tomato plants of cultivar RT on day 8 (A) and cultivar S on day 8 (B). MS chromatograms (m/z 100–1100) were acquired in ESI-negative mode. Retention times (in min) and accurate masses of the most intense signals are indicated in the chromatograms (plotted as base peak intensities [BPI], from 0 to 30 min). Black box: Highlighting the quantitative difference of a single metabolite (Rt = 14.7 min) between different treatments.*

*Figure S2.2: Negative ion mode background subtracted MS spectrum of putatively identified acetyl tryptophan (m/z =245.084) at Rt=13.91 min.*

### 2.2    Tryptophan derivatives

*Figure S2.3: Box-and-whiskers plots showing the relative concentrations of acetyl tryptophan at (A) day 8 and at (B) day 35 in plants of different treatment groups and cultivars.*

### 2.3    Hydroxycinnamic acids and chlorogenic acids (CGAs)

*Figure S2.4: Negative ion mode MS/MS spectra of the different caffeoylquinic acid isomers (m/z = 353) found to contribute to the variance between treatment groups. (A) 3-O-caffeoylquinic acid at Rt = 7.89 min, (B) 5-O-(E)-caffeoylquinic acid at Rt = 10.58 min, (C) 4-O-(Z)-caffeoylquinic acid at Rt = 11.09 min and (D) 5-O-(Z)-caffeoylquinic acid at Rt = 12.24 min.*

*Figure S2.5: Negative ion mode MS/MS spectrum of 5-O-(E)-feruloylquinic acid (m/z = 367.095) at Rt = 13.41 min.*

*Figure S2.6: Negative ion mode MS/MS spectrum of 5-O-(E)-caffeoylgalactaric acid (m/z = 371.053) at Rt = 7.77 min.*

*Figure S2.7: Negative ion mode MS/MS spectrum of 5-O-(E)-caffeoylquinic acid dimer (m/z = 707.181) at Rt = 10.7 min.*

**Figure S2.8:** *Negative ion mode MS/MS spectrum of 5-O-(E)-feruloylquinic acid (m/z = 735.211) at Rt = 13.53 min.*

**Figure S2.9:** *Negative ion mode MS/MS spectrum of 5-O-(E)-caffeoylgalactaric acid dimer (m/z = 743.129) at Rt = 7.78 min.*

**Figure S2.10:** *Box-and-whiskers plots showing the relative concentrations of (A) quinic acid (Rt = 10.59 min) and (B) galactaric acid (Rt = 7.79 min) in plants of different treatment groups and cultivars on day 8.*

**Figure S2.11:** *Box-and-whiskers plots showing the relative concentrations of (A) 5-O-(E)-caffeoylquinic acid (Rt = 10.59 min), (B) 5-O-(Z)-caffeoylquinic acid (Rt = 12.24 min), (C) 5-O-(E)-feruloylquinic acid (Rt = 13.41 min) and (D) 5-O-(E)-caffeoylgalactaric acid (Rt = 7.77 min) in plants of different treatment groups and cultivars on day 8.*

**Figure S2.12:** *Box-and-whiskers plots showing the relative concentrations of (A) 3-O-caffeoylquinic acid (Rt = 7.89 min), (B) 4-O-(Z)-caffeoylquinic acid (Rt = 11.09 min), (C) 5-O-(Z)-caffeoylquinic acid (Rt = 12.24 min), (D) 5-O-(E)-feruloylquinic acid (Rt = 13.41 min) and (E) 5-O-(E)-caffeoylgalactaric acid (Rt = 7.77 min), in plants of different treatment groups and cultivars on day 35.*

## 2.4 Phenolics

**Figure S2.13:** *Negative ion mode MS/MS spectra of (A) 2,3-dihydroxybenzoic-3-O-β-D-xyloside (m/z = 285.053) and (B) 2,3-dihydroxybenzoic-3-O-β-D-xyloside dimer (m/z = 571.125), both at Rt = 8.25 min, found to contribute to the variance between treatment groups.*

**Figure S2.14:** *Box-and-whiskers plots showing the relative concentrations of 2,3-dihydroxybenzoic-3-O-β-D-xyloside (Rt = 8.25 min) in plants of different treatment groups and cultivars at (A) day 8 and (B) day 35.*

**Figure S2.15:** *Negative ion mode MS/MS spectrum of sinapoylglycoside (m/z = 385.179) at Rt = 13.3 min, showing loss of 162 Da characteristic of a glucose residue forming m/z = 223.078 characteristic of sinapic acid.*

**Figure S2.16:** *Negative ion mode MS/MS spectrum of sinapoylglycoside FA (m/z = 431.185) at Rt = 13.3 min.*

**Figure S2.17:** *Box-and-whiskers plot showing the relative concentrations of sinapoylglycoside (Rt = 13.3 min) in plants of different treatment groups and cultivars on day 8.*

**Figure 2.18:** *Negative ion mode MS/MS spectrum of benzyl alcohol-hexose-pentose (m/z = 401.137) at Rt = 12.49 min.*

**Figure S2.19:** *Negative ion mode MS/MS spectrum of benzyl alcohol-hexose-pentose FA (m/z = 447.144) at Rt = 12.57 min.*

**Figure S2.20:** *Box-and-whiskers plots showing the relative concentrations of benzyl alcohol-hexose-pentose (Rt = 12.49 min) in plants of different treatment groups and cultivars at (A) day 8 and (B) day 35.*

## 2.5 Flavonols

**Figure S2.21:** *Negative ion mode MS/MS spectrum of (A) rutin (m/z = 609.141) at Rt = 16.66 min with (B) an enlarged image of (A) $[Y_0\text{-H}]^-$: $\overline{Y_0}$ ratio. Negative ion mode MS/MS spectrum of (C) quercetin-3-O-deoxyhexose-O hexose-O-pentose (m/z = 741.188) at Rt = 15.59 min with (D) an enlarged image of (C) $[Y_0\text{-H}]^-$: $\overline{Y_0}$ ratio.*

**Figure S2.22:** *Negative ion mode MS/MS spectrum of quercetin-3-rutinoside-7-glycoside (m/z = 771.197) at Rt = 12.76 min.*

**Figure S2.23:** *Box-and-whiskers plots showing the relative concentrations of (A) rutin (Rt = 16.66 min) and (B) quercetin-3-O-deoxyhexose-O-hexose-O-pentose acid (Rt = 15.59 min) in plants of different treatment groups and cultivars on day 8.*

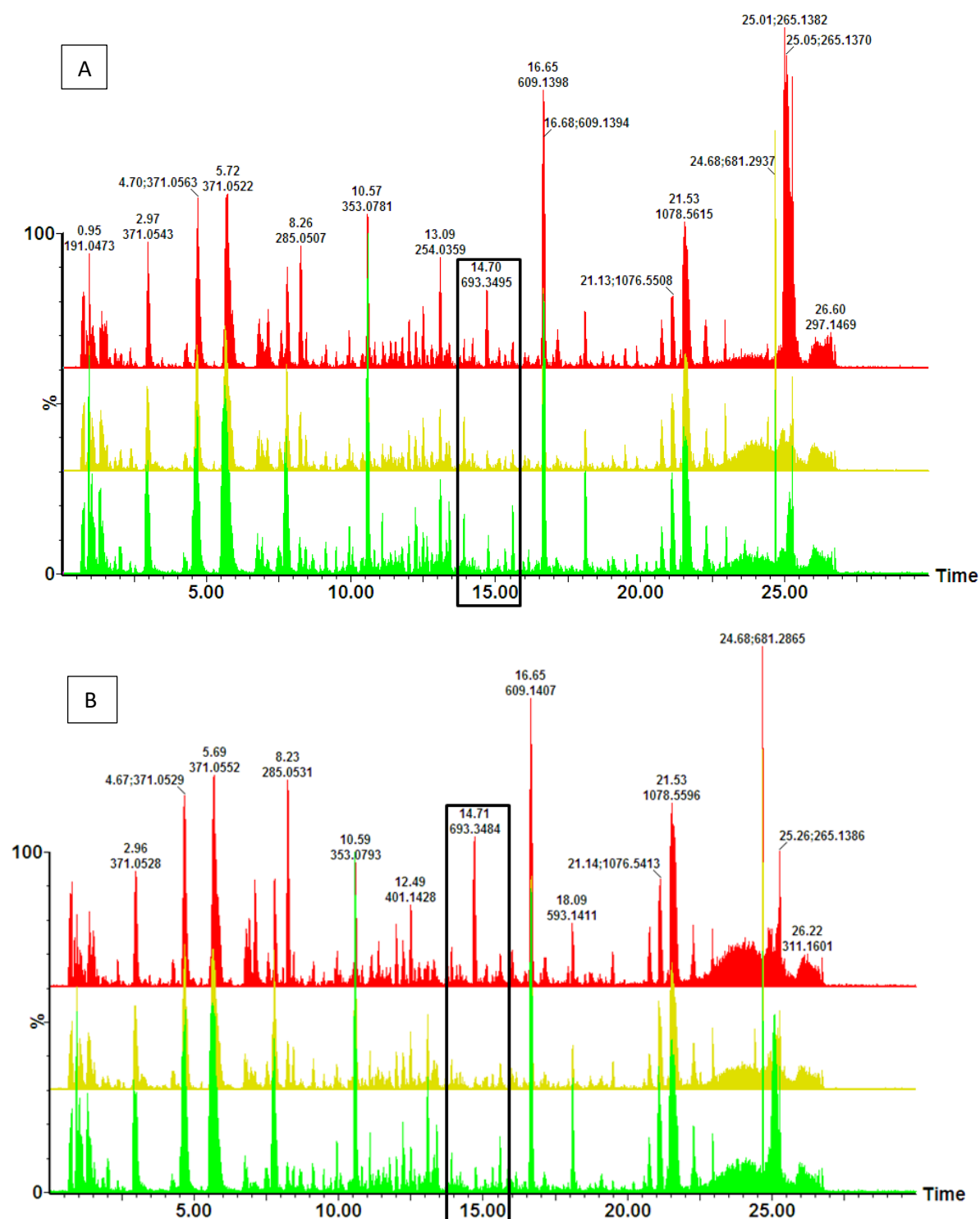## 2.1 UHPLC-HD-ESI-MS chromatograms of methanol extracts from tomato leaf tissue



**Figure S2.1 A** and **B:** Overlay of representative original chromatograms obtained by UHPLC-HD-ESI-MS of aqueous methanol extracts from tomato leaf tissue of Control (green), whitefly treated (yellow) and viruliferous whitefly treated (red) tomato plants of cultivar **RT** on day 8 (**A**) and cultivar **S** on day 8 (**B**). MS chromatograms (m/z 100–1100) were acquired in ESI-negative mode. Retention times (in min) and accurate masses of the most intense signals are indicated in the chromatograms (plotted as base peak intensities [BPI], from 0 to 30 min). Black box: Highlighting the quantitative difference of a single metabolite (Rt = 14.7 min) between different treatments.

## 2.2    Tryptophan derivatives

A compound with a precursor ion *m/z* = 245.084 at Rt = 13.91 min was putatively identified, by its MS spectrum (**Figure S**), as acetyl tryptophan due to the presence of an ion peak at *m/z* = 203.066, corresponding to tryptophan. The presence of acetyl tryptophan was previously reported in tomato seedlings (Roldan *et al.*, 2014).
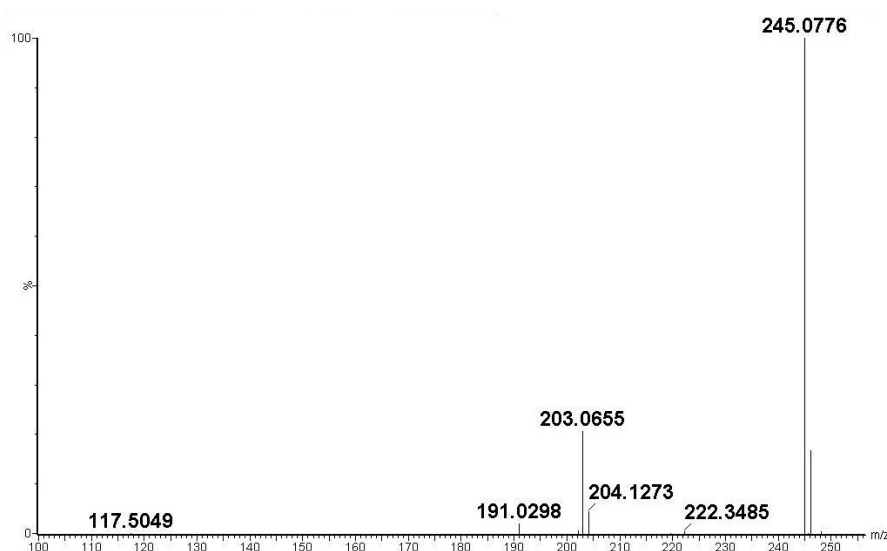


***Figure S2.2:*** *Negative ion mode background subtracted MS spectrum of putatively identified acetyl tryptophan (m/z =245.084) at Rt=13.91 min.*

Products of the tryptophan pathway are metabolised into a wide variety of compounds, such as auxin, glucosinolates, phytoalexins, alkaloids and other indolic compounds. These compounds play diverse roles in plant-pathogen interactions (López-Gresa *et al.*, 2012). Thus the increase in concentration in the **RT** and **S WF** treated groups, seen in **Figure S2.3**, most likely indicates an increase in acetyl tryptophan synthesis in response to whitefly feeding. The levels of this metabolite are lower in the **WF S** plants than in the **WF RT** plants possibly because the **S** plants are synthesising less acetyl tryptophan or because the **S** plants are rapidly using it as a precursor for other compounds. A slight further decrease in concentration in the **S WF+Vir** treated group is seen, while a significant decrease is seen in **RT WF+Vir** plants (compared to **RT WF** plants), this indicates that the acetyl tryptophan is likely being used to synthesise stress-response metabolites. In a study of the effects of Tomato mosaic virus (*ToMV*) on the metabolome of tomatoes it was found that in systemically infected leaves the levels of tryptophan increased, while they decreased in locally infected leaves (López-Gresa *et al.*, 2012).

On day 35 it is seen that the levels of acetyl tryptophan have evened out across different treatment groups for the **RT** cultivar, with it being very slightly elevated in the **WF** treated group. The levels of acetyl tryptophan in the **WF** treated and **WF+Vir** treated groups being more similar to that in the Con group supports the trend seen in the PCA scores plots of **RT** in which the different treatment groups do not cluster together but are blended, indicating the return of the **WF** and **WF+Vir** treated groups to homeostasis. The levels of acetyl tryptophan are also seen to have become more similar, by day 35, between different treatment groups of **S**.

Acetyl tryptophan therefore does not contribute to the separate clustering of the **WF+Vir** group seen in the PCA scores plot of **S** on day 35.

It is noted in **Figure S2.3** that the levels of acetyl tryptophan in the **RT** control group are much higher than that of the **S** control group both on day 8 and on day 35, indicating that the **RT** cultivar produces a larger amount of acetyl tryptophan constitutively, thus leading to a larger pool of tryptophan being available for use in synthesis of defence compounds when needed, possibly allowing the **RT** cultivar to respond to the stress much more quickly than the **S** cultivar.
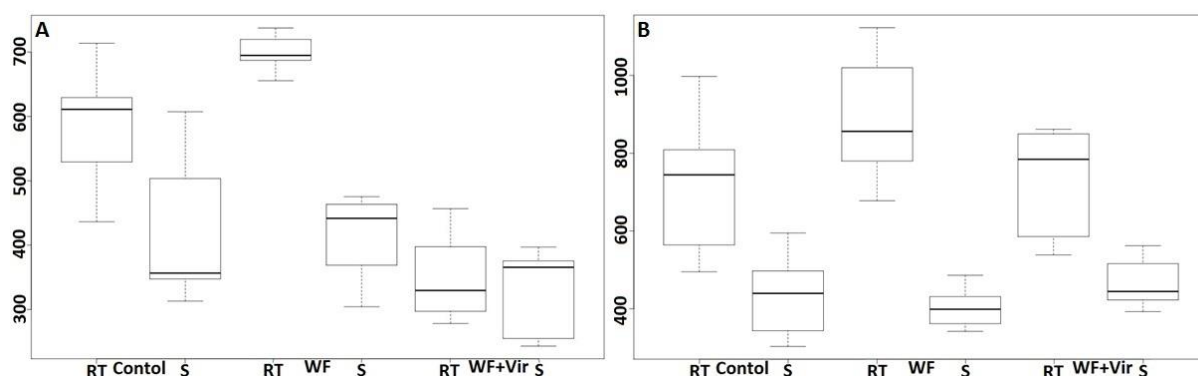


***Figure S2.3:*** *Box-and-whiskers plots showing the relative concentrations of acetyl tryptophan at (A) day 8 and at (B) day 35 in plants of different treatment groups and cultivars.*

## 2.3 Hydroxycinnamic acids and chlorogenic acids (CGAs)

Three compounds with precursor ions ([M-H]⁻) $m/z$ = 163.032, 191.047 and 209.021 were identified using their MS spectra, as well as their Rts, as quinic acid, *p*-coumaric acid and galactaric acid, respectively. Other important precursor molecules of CGAs, such as caffeic acid and ferulic were not found to contribute significantly to variation between different treatment groups. However, these compounds are able to join in different combinations to give a variety of CGAs. Using the MS/MS spectra of the compounds with precursor ions [M-H]⁻ of $m/z$ = 353, 367.095 and 371.053, they were identified as caffeoylquinic acid, feruloylquinic acid and caffeoylgalactaric acid respectively.

Positional as well as geometrical isomers of each of these CGAs exist and different isomers of caffeoylquinic acids could be distinguished using a hierarchical key on how to discriminate between caffeoylquinic acid isomers (Clifford *et al.,* 2005). Four isomers of caffeoylquinic acid were identified, 3-*O*-caffeoylquinic acid at Rt = 7.89 min, 5-*O*-(E)-caffeoylquinic acid at Rt = 10.58 min, 4-*O*-(Z)-caffeoylquinic acid at Rt = 11.09 min and 5-*O*-(Z)-caffeoylquinic acid at Rt = 12.24 min.

The MS/MS spectrum of the precursor ion $m/z$ = 353.079 at Rt = 7.89 min (**Figure S2.4**) shows the presence of a base peak at $m/z$ = 191.051 and a peak of approximately 50% intensity at $m/z$ = 179.029; indicating the ester bond at position 3 on the quinic acid. The MS/MS spectrum of the precursor ion $m/z$ = 353.078 at Rt = 10.58 min (**Figure S2.4**) shows the presence of a base peak at $m/z$ = 191.038 along with a very weak ion peak at $m/z$ = 178.997. This indicates that the ester bond between caffeic acid and quinic acid at the 5 position of the quinic acid ring. The presence of the base peak at $m/z$ = 173.031 on the MS/MS spectrum of $m/z$ = 353.080 at

Rt = 11.09 min (**Figure S2.4**) indicates that the ester bond is at position 4 of the quinic acid ring (Ncube et al., 2014). On the MS/MS spectrum of the precursor ion *m/z* = 353.080 at Rt = 12.24 min (**Figure S2.4**), a base peak is seen at *m/z* = 191.042 along with an extremely weak ion peak at *m/z* = 178.909, indicating the presence of the ester bond at position 5 of the quinic acid ring. In order to distinguish between *cis-* and *trans*-isomers of 5-*O*-caffeoylquinic acids, the Rt of each was considered. Clifford *et al.* (2008) found that *cis*-5-acyl isomers were more hydrophobic than their *trans* counterparts, thus the *trans* isomers would elute from the reverse phase column before the *cis* isomers meaning that the 5-*O*-caffeoylquinic acid at Rt = 10.58 min would be the *trans* isomer while the 5-*O*-caffeoylquinic acid at Rt = 12.24 min would be the *cis* isomer.
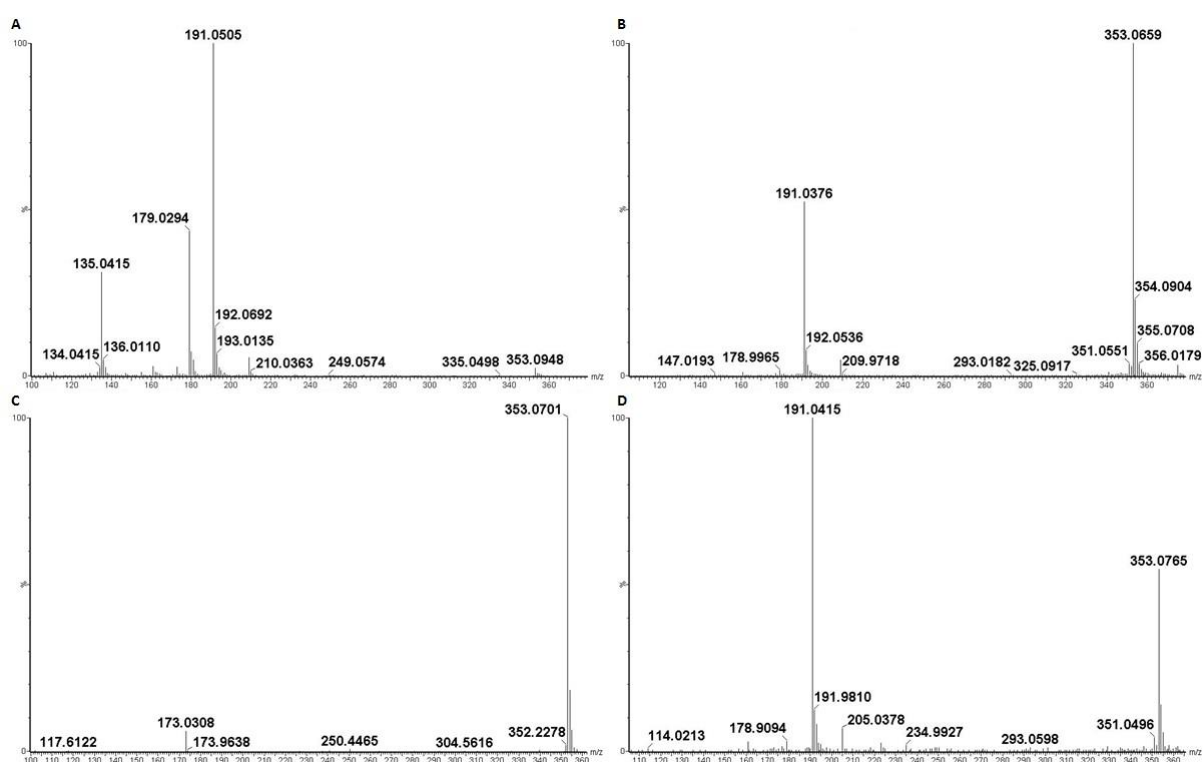


**Figure S2.4:** *Negative ion mode MS/MS spectra of the different caffeoylquinic acid isomers (m/z = 353) found to contribute to the variance between treatment groups. (A) 3-O-caffeoylquinic acid at Rt = 7.89 min, (B) 5-O-(E)-caffeoylquinic acid at Rt = 10.58 min, (C) 4-O-(Z)-caffeoylquinic acid at Rt = 11.09 min and (D) 5-O-(Z)-caffeoylquinic acid at Rt = 12.24 min.*

The MS/MS spectrum of the precursor ion *m/z* = 367.095 at Rt = 13.41 min (**Figure S2.5**) shows the presence of a base peak at *m/z* = 191.049. According to the hierarchical scheme for identifying CGAs set out by Clifford *et al.* (2003), this indicates that this metabolite is 5-*O*-feruloylquinic acid.
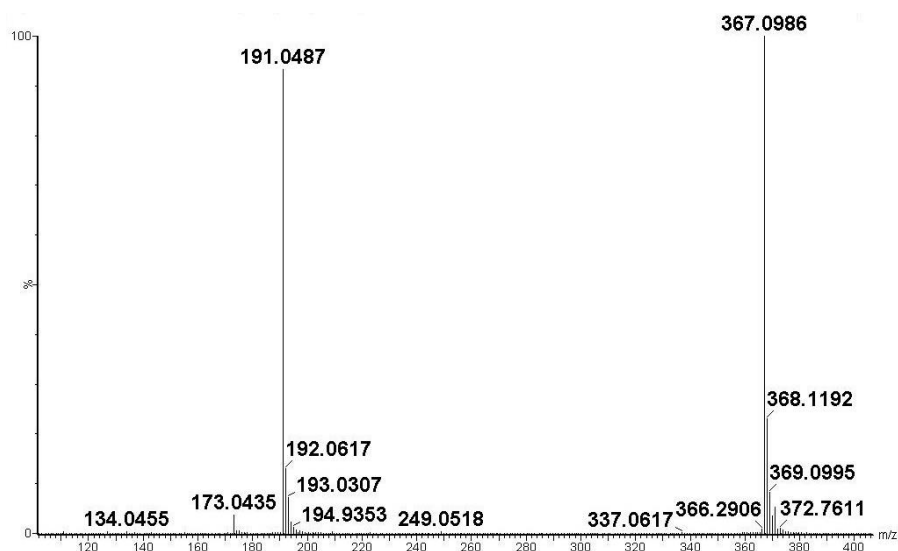
***Figure S2.5:*** *Negative ion mode MS/MS spectrum of 5-O-(E)-feruloylquinic acid (m/z = 367.095) at Rt = 13.41 min.*

The MS spectrum of the precursor ion *m/z* = 371.053 at Rt = 7.77 min (**Figure S2.6**) shows the presence of a base peak at *m/z* = 209.012 which is characteristic of caffeoylgalactaric acid. The presence of a smaller peak at *m/z* = 191.007 and a much smaller peak at *m/z* = 178.999 indicates that it is a 5 positional isomer, *i.e.* 5-*O*-caffeoylgalactaric acid. It has previously been found that the major geometrical isomer of 5-*O*-caffeoylgalactaric acid found in tomato is the *trans* isomer.
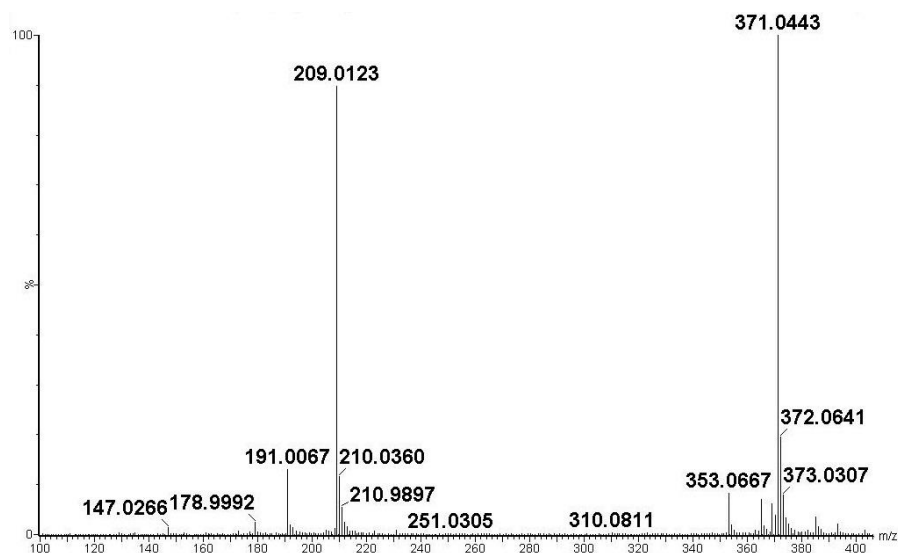


***Figure S2.6:*** *Negative ion mode MS/MS spectrum of 5-O-(E)-caffeoylgalactaric acid (m/z = 371.053) at Rt = 7.77 min.*

The MS spectrum of the precursor ion *m/z* = 707.181 at Rt = 10.7 min (**Figure S2.7**) shows the presence of a base peak at *m/z* = 353.066, a much less intense peak at *m/z* = 191.037 and a very weak ion peak at *m/z* = 179.027. These peaks along with the Rt indicate that this compound is a dimer of 5-*O*-(E)-caffeoylquinic acid.
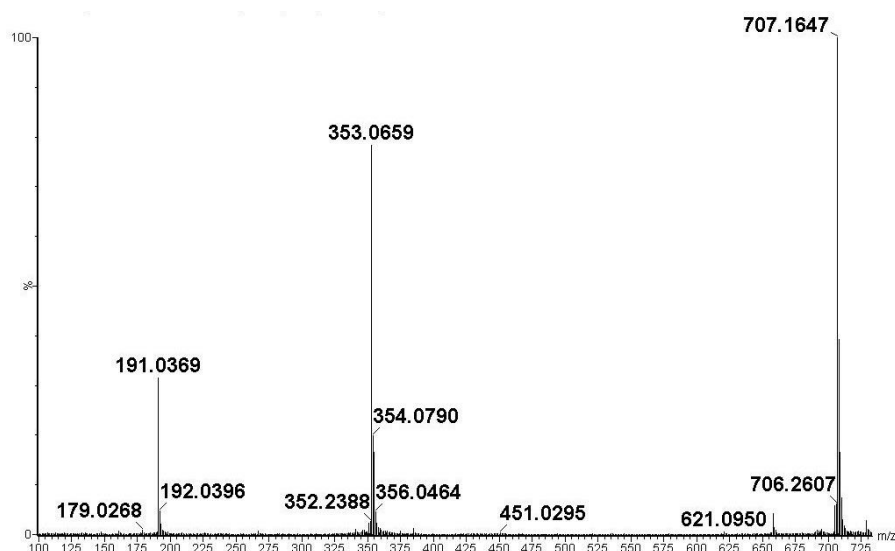
*Figure S2.7: Negative ion mode MS/MS spectrum of 5-O-(E)-caffeoylquinic acid dimer (m/z = 707.181) at Rt = 10.7 min.*

The MS spectrum of the precursor ion *m/z* = 735.211 at Rt = 13.53 min (**Figure S2.8**) shows the presence of a base peak at *m/z* = 367.086, a much less intense peak at *m/z* = 191.036 and a very weak ion peak at *m/z* = 173. These peaks along with the Rt indicate that this compound is a dimer of 5-*O*-(E)-feruloylquinic acid.
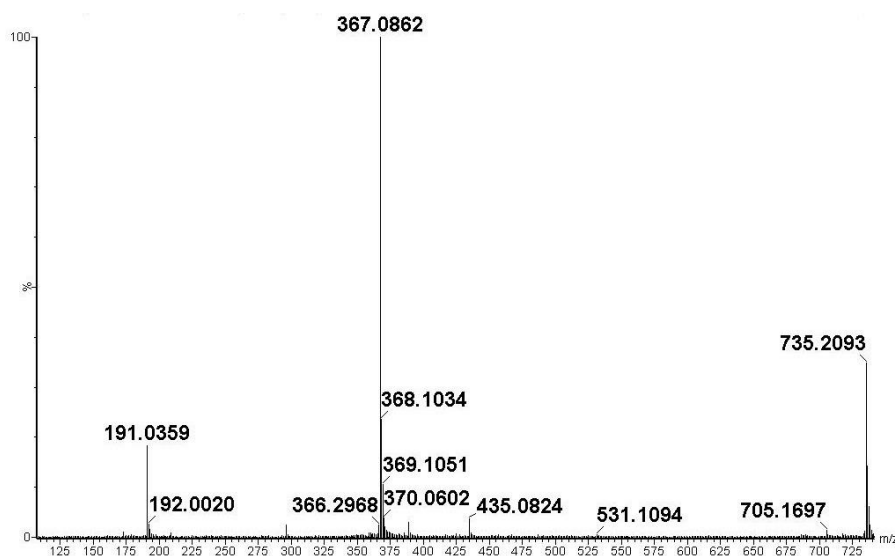


*Figure S2.8: Negative ion mode MS/MS spectrum of 5-O-(E)-feruloylquinic acid (m/z = 735.211) at Rt = 13.53 min.*

The MS spectrum of the precursor ion *m/z* = 743.129 at Rt = 7.78 min (**Figure S2.9**) shows the presence of a base peak at *m/z* = 371.042, an intense peak at *m/z* = 209.013, a weak ion peak at *m/z* = 191 and a very weak ion peak at *m/z* = 179. These peaks along with the Rt indicate that this compound is a dimer of 5-*O*-(E)-caffeoylgalactaric acid.
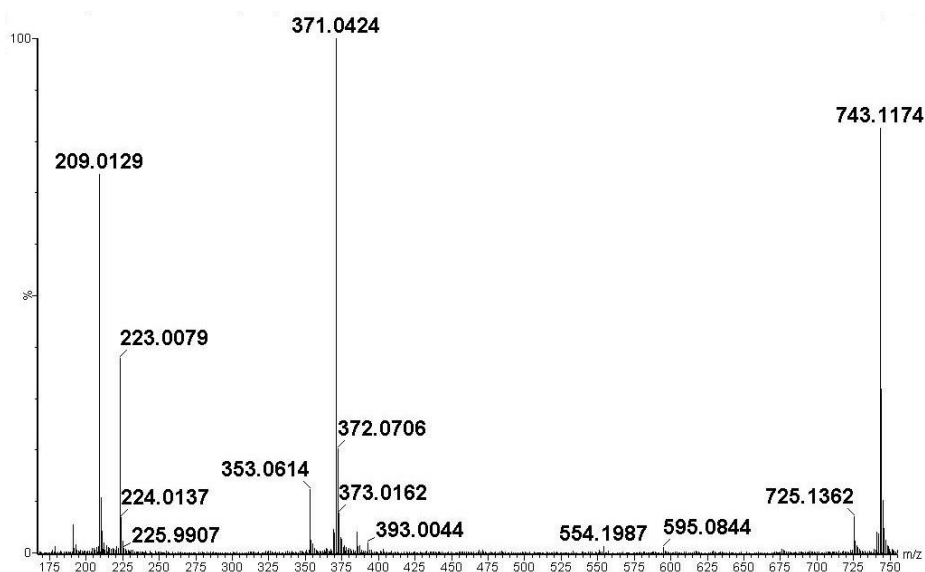
***Figure S2.9:*** *Negative ion mode MS/MS spectrum of 5-O-(E)-caffeoylgalactaric acid dimer (m/z = 743.129) at Rt = 7.78 min.*

**Figure S2.10** shows the box-and-whiskers plots of the relative concentrations of quinic acid (QA) (**Figure S2.10**) and galactaric acid (GA) (**Figure S2.10**) while

**Figure S2.11** shows the relative levels of 5-*O*-(E)-caffeoylquinic acid (

**Figure S2.11**), 5-*O*-(Z)-caffeoylquinic acid (

**Figure S2.11**), 5-*O*-(E)-feruloylquinic acid (

**Figure S2.11**) and that of 5-*O*-(E)-caffeoylgalactaric acid (

**Figure S2.11**). The levels of the QA and GA esters (QAE and GAE) (

**Figure S2.11**) are noted to follow the same pattern of their precursor metabolite (QA and GA) levels seen in

**Figure S2.10**. This is likely due to the precursor metabolites being used to replenish the QAE and GAE in **WF** and **WF+Vir** treated plants after their initial decrease (due to feeding and infection) or possibly due to a redirection of resources to other defence metabolites. It was observed that the relative levels of both QA and GA (**Figure S2.10**2.10) and the resulting esters (

**Figure S2.11**2.11) on day 8 were lower in the **WF** and the **WF+Vir** treated groups of both the **RT** and **S** cultivars compared to the levels in the control group.

The levels of each of the aforementioned QAE and GAE, as well as their precursors were slightly higher in the **WF** treated groups than they were in the **WF+Vir** treated groups for both cultivars, indicating that whitefly feeding has a large effect on the QA and GA levels and the levels of the corresponding esters of the host plant. It is also noted that for each cultivar, viral infection decreased the levels of QA / QAE and GA / GAE. This further decrease could be due to resources being redirected toward other defence compounds. The levels of QA and GA and the QAE and GAE in the control groups of the **RT** cultivar are lower than that in the **S** cultivar; suggesting that the **S** cultivar, under normal circumstances, produces a higher constitutive amount of QA and GA and therefore QAE and GAE compared to the **RT** cultivar. This is also seen to be the case when comparing the **WF** treated groups of the **RT** and the **S** cultivar, *i.e.* the precursor and ester levels in the **S** cultivar are higher than

that of the **RT** cultivar, perhaps due to the lower constitutive levels of these metabolites in the **RT** cultivar. This trend however is not apparent when comparing the **WF+Vir** treated groups of the **RT** and the **S** cultivar, where it is seen that the ester levels in the **WF+Vir** treated **RT** cultivar are higher than those in the **S** cultivar.
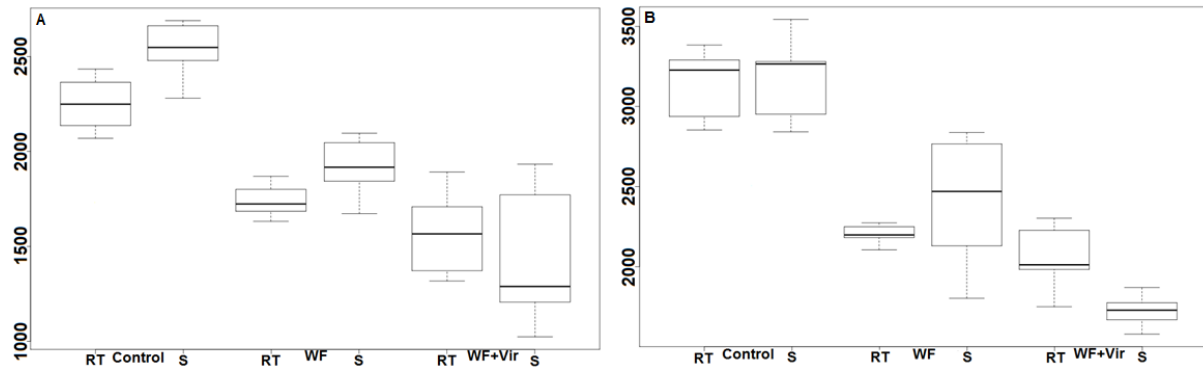


*Figure S2.10:* Box-and-whiskers plots showing the relative concentrations of (A) quinic acid (Rt = 10.59 min) and (B) galactaric acid (Rt = 7.79 min) in plants of different treatment groups and cultivars on day 8.
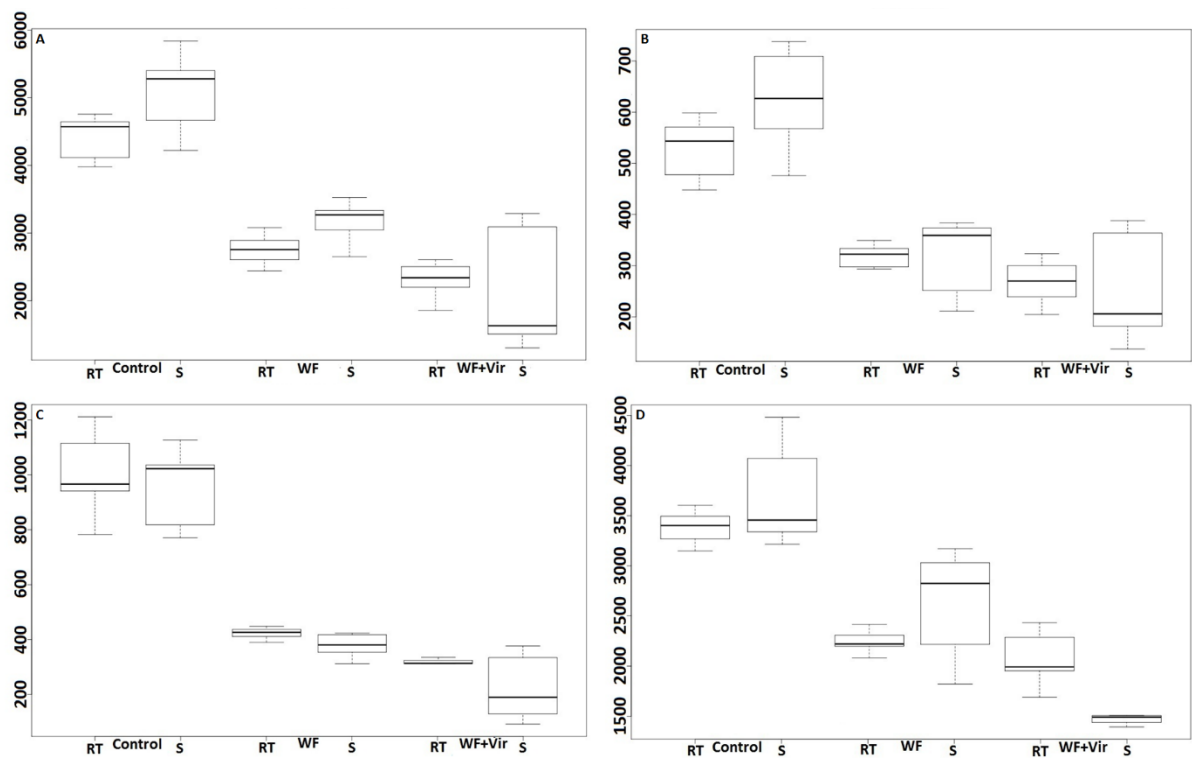


*Figure S2.11:* Box-and-whiskers plots showing the relative concentrations of (A) 5-O-(E)-caffeoylquinic acid (Rt = 10.59 min), (B) 5-O-(Z)-caffeoylquinic acid (Rt = 12.24 min), (C) 5-O-(E)-feruloylquinic acid (Rt = 13.41 min) and (D) 5-O-(E)-caffeoylgalactaric acid (Rt = 7.77 min) in plants of different treatment groups and cultivars on day 8.

The notable decrease of the QAE and GAE (Figure S2.11) was unexpected, as whitefly feeding induces a salicylic acid increase in the host plant which, in turn, has been found to increase. The most likely explanation is that this decrease is due to whitefly ingestion of CGAs, as CGAs are present in the phloem making their ingestion unavoidable, and redirection of the phenylpropanoid pathway occurring simultaneously. It is seen on day 35 (Figure S2.12) that CGA levels in **WF** treated plants had not fully returned to that of the controls, most likely indicating that the whitefly feeding induced a long term redirection of the phenylpropanoid pathway toward other defence compounds.
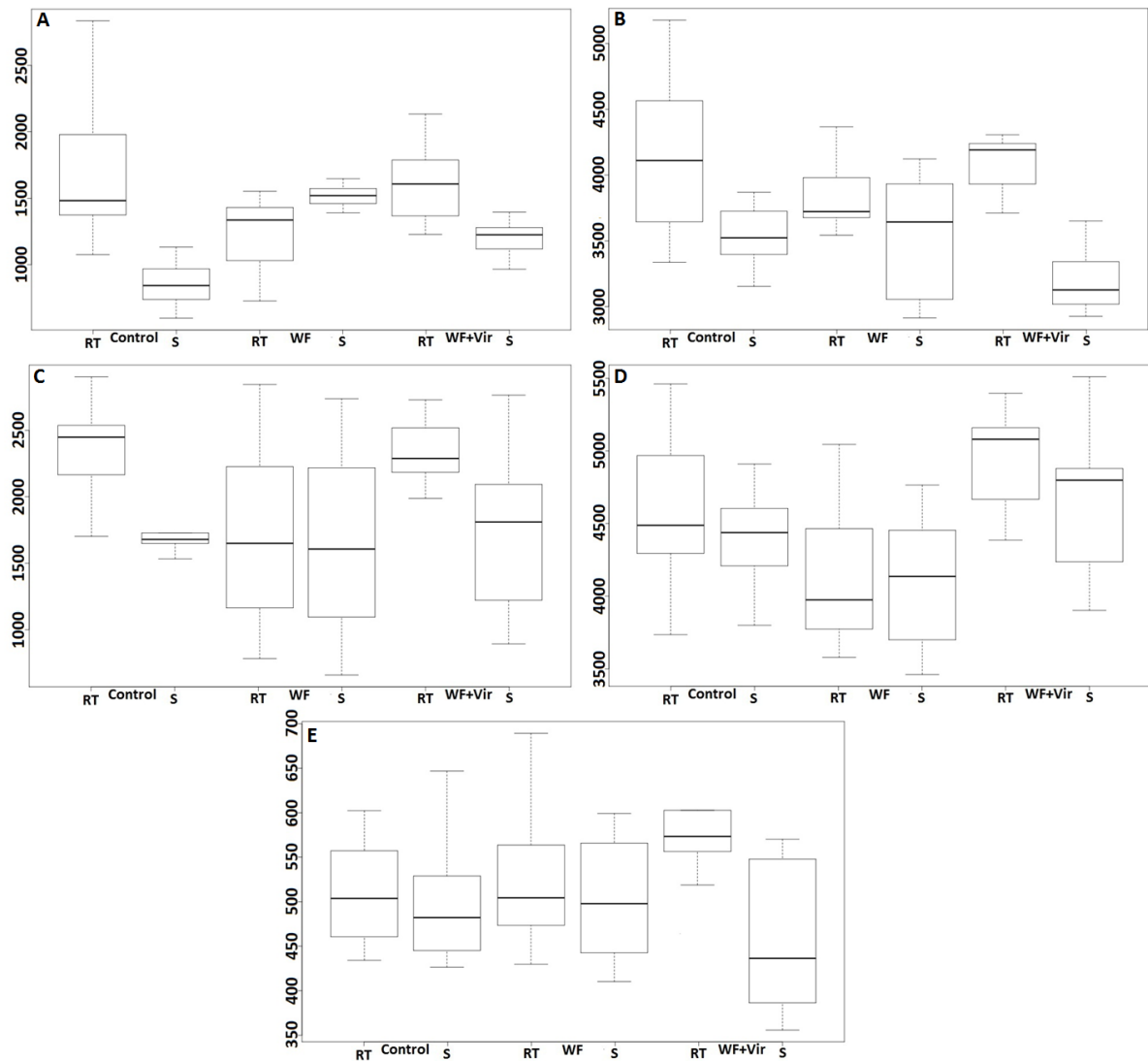


*Figure S2.12: Box-and-whiskers plots showing the relative concentrations of (A) 3-O-caffeoylquinic acid (Rt = 7.89 min), (B) 4-O-(Z)-caffeoylquinic acid (Rt = 11.09 min), (C) 5-O-(Z)-caffeoylquinic acid (Rt = 12.24 min), (D) 5-O-(E)-feruloylquinic acid (Rt = 13.41 min) and (E) 5-O-(E)-caffeoylgalactaric acid (Rt = 7.77 min), in plants of different treatment groups and cultivars on day 35.*

The overall concentration of the 5-*O*-(E)-caffeoylquinic acid dimer is higher than that of the 5-*O*-(E)-caffeoylquinic acid monomer while the overall concentration of the 5-*O*-(E)-caffeoylgalactaric acid dimer is lower than that of the 5-*O*-(E)-caffeoylgalactaric acid monomer. Otherwise the same trend in concentrations is seen between different treatment groups and different cultivars. Dimer levels observed do not necessarily reflect those present in the plants, as dimers can form during MS analysis.

## 2.4 Phenolics

The precursor ion *m/z* = 285.053 at Rt = 8.25 min was identified as 2,3-dihydroxybenzoic-3-*O*-β-D-xyloside. The MS/MS spectrum (**Figure S2.13A**) showed the presence of a peak at *m/z* = 285.053 and another more intense peak at *m/z* = 152, the difference of 132 Da corresponding to the loss of a xyloside residue. A base peak was observed at *m/z* = 108 indicating the loss of 44 Da corresponding to $CO_2^-$. A dimer of this molecule was observed at the same Rt with precursor ion *m/z* = 571.125. The MS/MS spectrum of the precursor ion *m/z* = 571.125 (**Figure S2.13**), showed the presence of a base peak at *m/z* = 285.053, corresponding to the 2,3-dihydroxybenzoic-3-*O*-β-D-xyloside monomer molecule. A weak ion peak was observed at *m/z* = 153 along with a weaker ion peak at *m/z* = 109 corresponding to the loss of a xyloside residue and a subsequent loss of $CO_2^-$ respectively.
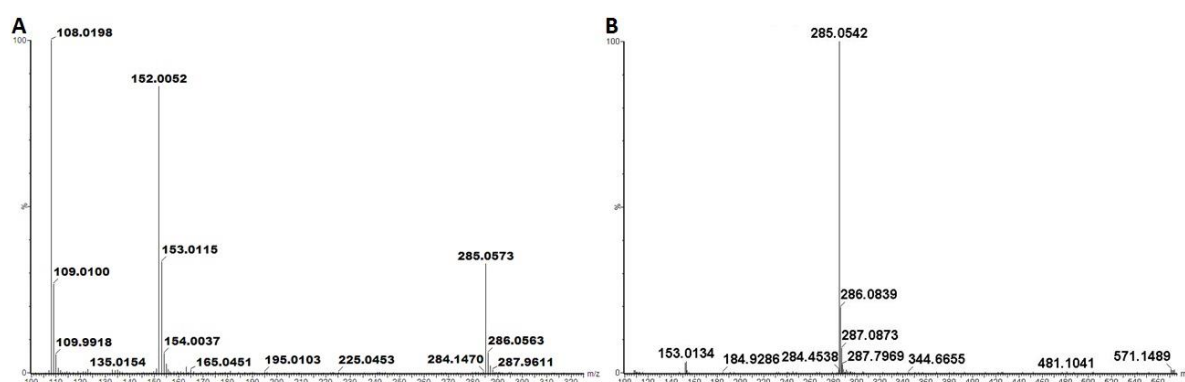


**Figure S2.13:** *Negative ion mode MS/MS spectra of (A) 2,3-dihydroxybenzoic-3-O-β-D-xyloside (m/z = 285.053) and (B) 2,3-dihydroxybenzoic-3-O-β-D-xyloside dimer (m/z = 571.125), both at Rt = 8.25 min, found to contribute to the variance between treatment groups.*

**Figure S2.14** shows the differing levels of 2,3-dihydroxybenzoic-3-*O*-β-D-xyloside (2,3-DHBX) found in different treatment groups of each cultivar on day 8 (**Figure S2.14A**) and on day 35 (**Figure S2.14B**). On day 8 the levels of 2,3-DHBX in the **RT WF** treated group are seen to be approximately the same as those in the **RT** control group, while the levels are seen to be much higher in the **WF+Vir** treated group of the **RT** cultivar. On day 35 the levels in the **RT** cultivar are seen to be slightly lower in the **WF** treated group than in the control group while the levels in the **WF+Vir** group are seen to be much higher. On day 8 the 2,3-DHBX levels were very low in the control group of the **S** cultivar, and slightly elevated in the **WF** treated group and drastically increased in the **WF+Vir** treated group (**Figure S2.14**). On day 35 the levels were seen to still be much higher in the **WF+Vir** treated group relative to the control group while the levels were approximately the same in the **WF** treated

group as in the control group. This is in support of the trend seen in the PCA scores plot indicating that the **WF** treated group and the control group of the **S** cultivar become more metabolically similar on day 35 but because all metabolites to do not return to control levels in the **WF** treated group on day 35 the two groups still remain separate.
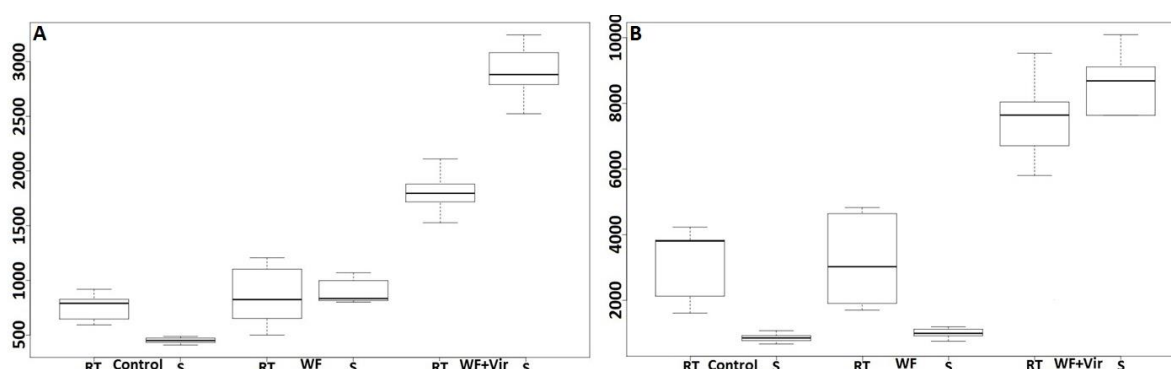


***Figure S2.14:*** *Box-and-whiskers plots showing the relative concentrations of 2,3-dihydroxybenzoic-3-O-ß-D-xyloside (Rt = 8.25 min) in plants of different treatment groups and cultivars at (A) day 8 and (B) day 35.*

The levels of 2,3-DHBX in the control group of the **RT** cultivar at both day 8 and day 35 were higher than those in the control group of the **S** cultivar at both day 8 and day 35. On day 8 the levels were approximately the same in **S WF** treated plants as they were in **RT WF** treated plants, on day 35 however the levels in the **S WF** treated plants had declined to match that of the **S** control group. The level in the **RT WF+Vir** treated group was much less than that in **S WF+Vir** on day 8, while on day 35 the **RT WF+Vir** levels were almost as high as those in the **S WF+Vir**.

A study found that 2,3-DHBA and its xylose conjugate 2,3-DHBX accumulated in aged and in *Pseudomonas syringae* pv. *tomato* inoculated Arabidopsis leaves. The majority of the accumulated 2,3-DHBA was found to be in the xylose conjugated form, 2,3-DHBX, which may serve as a reservoir of nonconjugated 2,3-DHBA. This compound can also be dehydroxylated to form SA, offering a mechanism to regulate SA levels.

It has previously been found that whitefly feeding induces SA defences and per implication, production of SA . Higher levels of SA accumulation have also been observed in pepper plants resistant to infection by two geminiviruses (*Pepper golden mosaic virus* and *Pepper huasteco yellow vein virus*), compared to their susceptible counterparts.  In light of this, it is possible that *ToCSV* infection caused an increase in SA accumulation in the **WF+Vir** plants, leading to the plant counteracting this event by converting excess SA to 2,3-DHBX.

**Figure S2.15** shows the MS/MS spectrum of the precursor ion $m/z$ = 385.179 at Rt = 13.30 min, identified as sinapoyl glycoside. From the spectrum a base peak is observed at $m/z$ = 153.088 and a slightly weaker ion peak at $m/z$ = 223.078, corresponding to deprotonated sinapic acid after the loss of 162 Da corresponding to a glycoside residue.
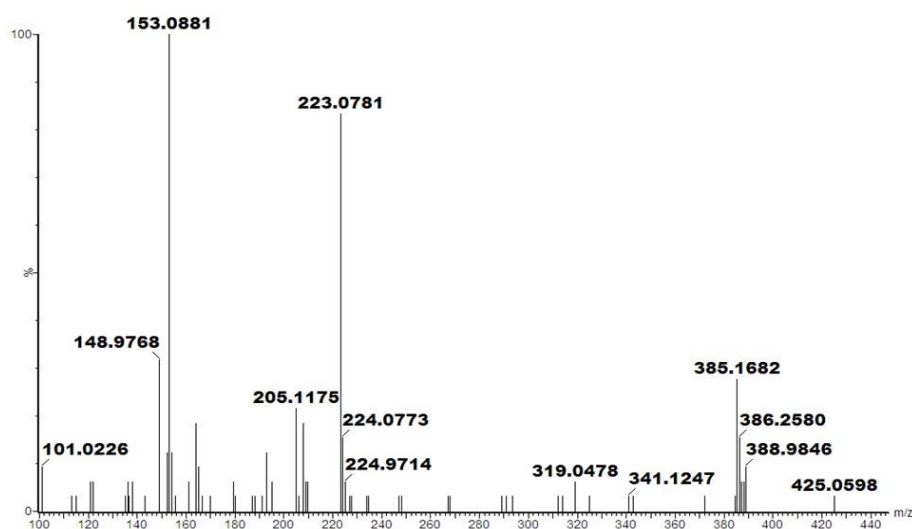
*Figure S2.15*: Negative ion mode MS/MS spectrum of sinapoylglycoside (m/z = 385.179) at Rt = 13.3 min, showing loss of 162 Da characteristic of a glucose residue forming m/z = 223.078 characteristic of sinapic acid.

The MS/MS spectrum of the compound with precursor ion *m/z* = 431.185 (**Figure S2.16**) was found to be very similar to that of the compound with precursor ion *m/z* = 385.179 (**Figure S2.15**). The difference between the precursor ion *m/z* = 431.185 and the base peak at *m/z* = 385.179 is 46 Da corresponding to deprotonated formic acid. Thus this compound is thought to be a formic acid adduct of sinapoylglycoside.
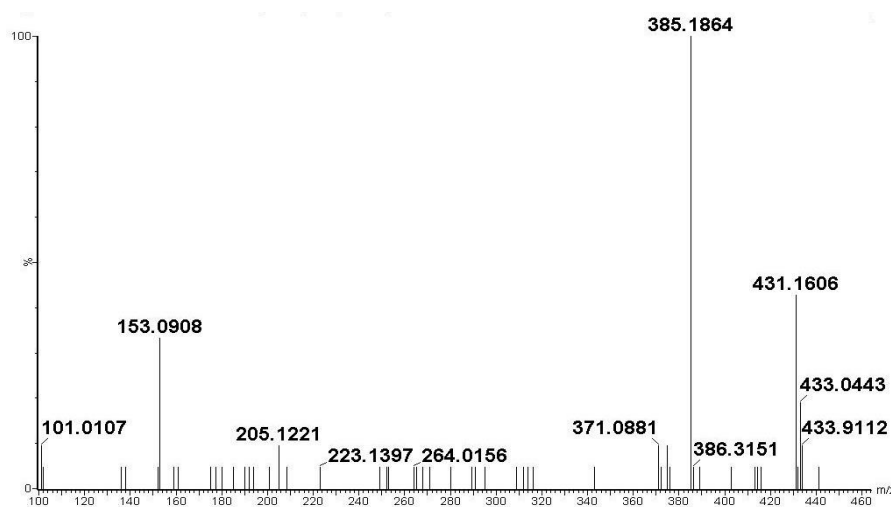


*Figure S2.16*: Negative ion mode MS/MS spectrum of sinapoylglycoside FA (m/z = 431.185) at Rt = 13.3 min

**Figure S2.17** shows the differing levels of sinapoylglycoside (*m/z* = 385.179) found in different treatment groups of each cultivar on day 8. The levels of sinapoylglycoside increased slightly after **WF** treatment of the **RT** cultivar on day 8, but decreased in the **WF+Vir** treated group. The levels of sinapoylglycoside were approximately the same in the **S** cultivar after **WF** treatment, but had decreased after **WF+Vir** treatment. The levels were higher in the **S** cultivar of the control group and the **WF** treated group, compared to that of the **RT** group. The levels in the **RT WF+Vir** group were however higher than the levels of the **S WF+Vir** treated group.
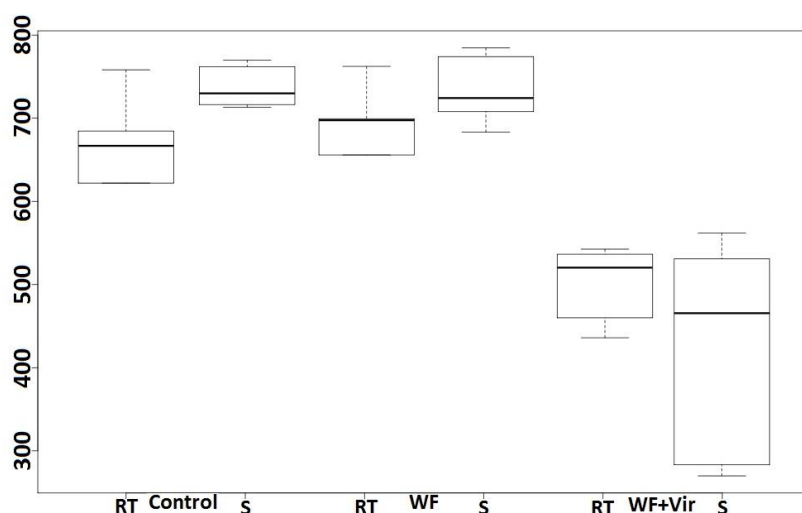
*Figure S2.17: Box-and-whiskers plot showing the relative concentrations of sinapoylglycoside (Rt = 13.3 min) in plants of different treatment groups and cultivars on day 8.*

Sinapoylglycoside was reported to be an activated sinapate donor and as such functions as the immediate precursor for other sinapate esters, such as sinapoylmalate, sinapoyl choline as well as 1,2 di-sinapoylglucose and sinapoylated anthocyanins. Sinapate esters, in particular sinapoylmalate has been described as stress metabolites.

The most likely explanation for the decrease in sinapoylglycoside levels seen in the **WF+Vir** treated groups is that viral infection causes the plants to redirect metabolic flow from formation of sinapoylglycoside to other defence products or polymers, such as lignin.

**Figure S2.18** shows the MS/MS spectrum of precursor ion $m/z$ = 401.137 at Rt = 12.49 min. The spectrum shows the presence of a base peak at $m/z$ = 269.087 corresponding to the loss of a pentose unit of 132 Da, leaving a benzyl alcohol glycoside.
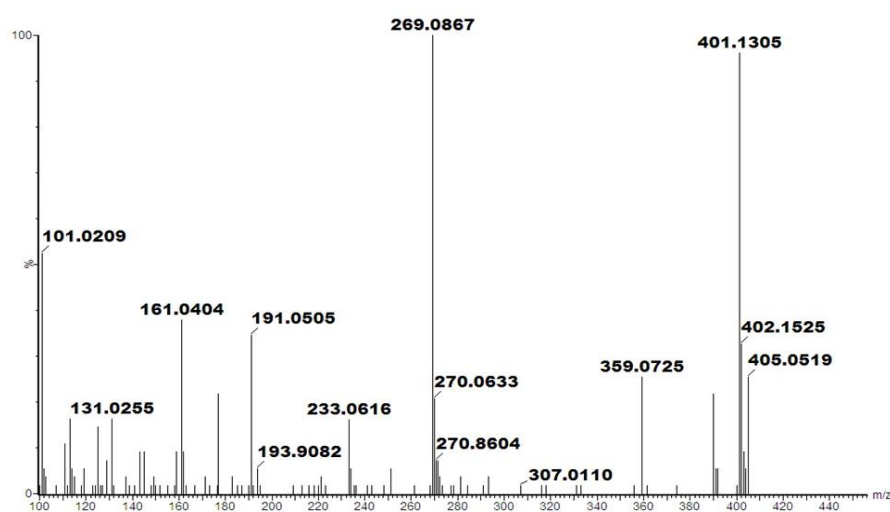


*Figure S2.18: Negative ion mode MS/MS spectrum of benzyl alcohol-hexose-pentose (m/z = 401.137) at Rt = 12.49 min.*

The MS/MS spectrum of the compound with precursor ion $m/z$ = 447.144 (**Figure S2.19**) was found to be very similar to that of the compound with precursor ion $m/z$ = 401.137 (**Figure S2.18**). The difference between the precursor ion $m/z$ = 447.144 and the base peak at $m/z$ = 401.137 is 46 Da corresponding to deprotonated formic acid. Thus this compound is thought to be a formic acid adduct of benzyl alcohol-hexose-pentose.
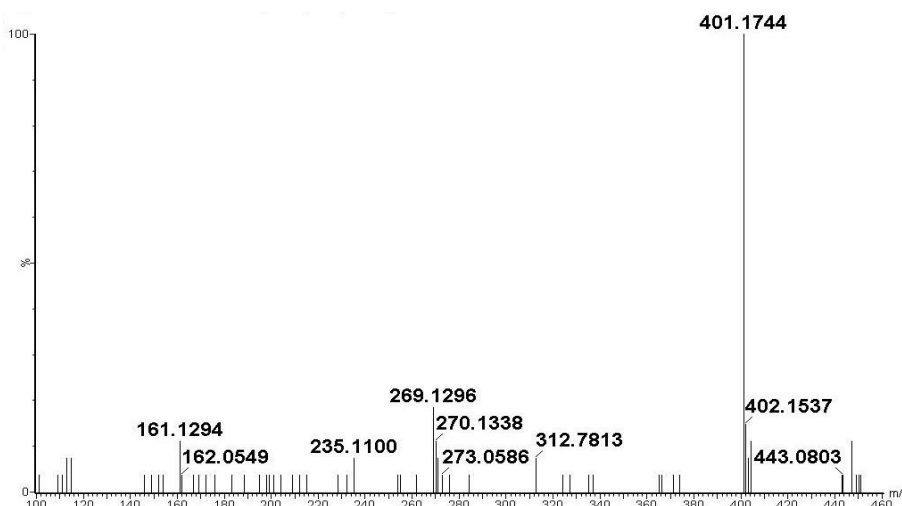


***Figure S2.19:*** *Negative ion mode MS/MS spectrum of benzyl alcohol-hexose-pentose FA (m/z = 447.144) at Rt = 12.57 min.*

Benzyl alcohol-hexose-pentose ($m/z$ = 401.137) was identified as a compound significantly contributing to the variance between different treatment groups of **RT** and **S** plants on day 8 and also on day 35 resulting in the clustering seen in the PCA scores plots. From **Figure S2.20A** it is seen that the relative levels of this compound, on day 8, increased slightly after **WF** treatment in both **S** and **RT** cultivars in comparison with their control groups.

The **WF** treated groups of the two cultivars show almost the same levels of this metabolite, with that in the **S** cultivar being slightly lower. In the **WF+Vir** treated groups of each cultivar this compound is seen to increase (compared to controls). On day 35 it is observed that the levels in the **WF** treated group of the **RT** cultivar had decreased compared to the control, while the level in the **WF** treated **S** cultivar is seen to be very similar to that of the **S** control. The **WF** treated groups of both cultivars also seem to have similar levels of the metabolite. It is expected that the level of this metabolite in the **WF** treated groups of both cultivars would become more similar to that of the control plants over time since the **WF** are removed on day 7. The levels of the metabolite are seen to have increased even more in **WF+Vir RT** and **S** on day 35 relative to the control than it did on day 8. Unlike on day 8, on day 35 the metabolite level is seen to be higher in the **WF+Vir S** cultivar than in the **WF+Vir RT** cultivar.
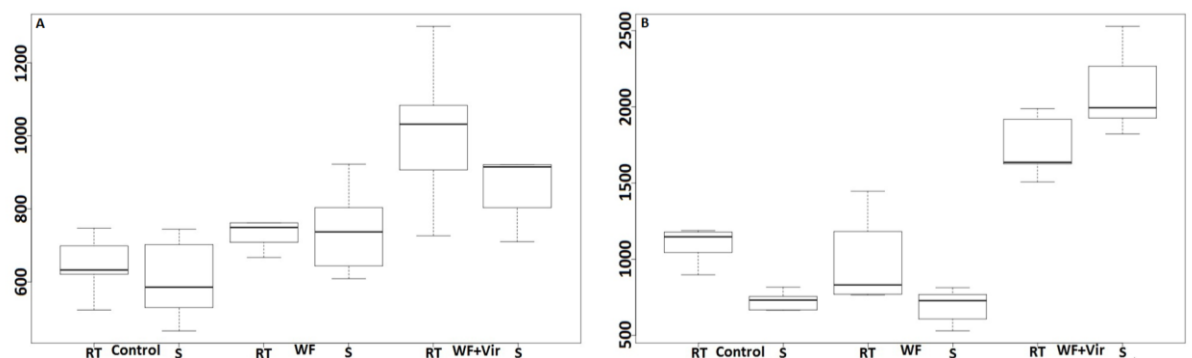
*Figure S2.20: Box-and-whiskers plots showing the relative concentrations of benzyl alcohol-hexose-pentose (Rt = 12.49 min) in plants of different treatment groups and cultivars at (A) day 8 and (B) day 35.*

Conjugated benzoic acid accumulated in tobacco after infection with tobacco mosaic virus, associated with a strong correlation between SA and conjugated benzoic acid levels, with the latter likely intermediates in SA synthesis. This information, together with the finding that whitefly feeding and infection with their vectored begomoviruses induce an increase in SA production, can explain the increase in benzyl alcohol-hexose-pentose levels in the **WF** and **WF+Vir** treated groups as a result of SA increase.

## 2.5 Flavonols

Three compounds with precursor ions $m/z$ = 609.141, $m/z$ = 741.188 and $m/z$ = 771.197 at Rt 16.66, 15.59 and 12.76 min respectively were identified, using their respective MS/MS spectra (**Figure S2.21A/C and Figure S2.22**), as glycosylated flavonols of the flavonoid quercetin.
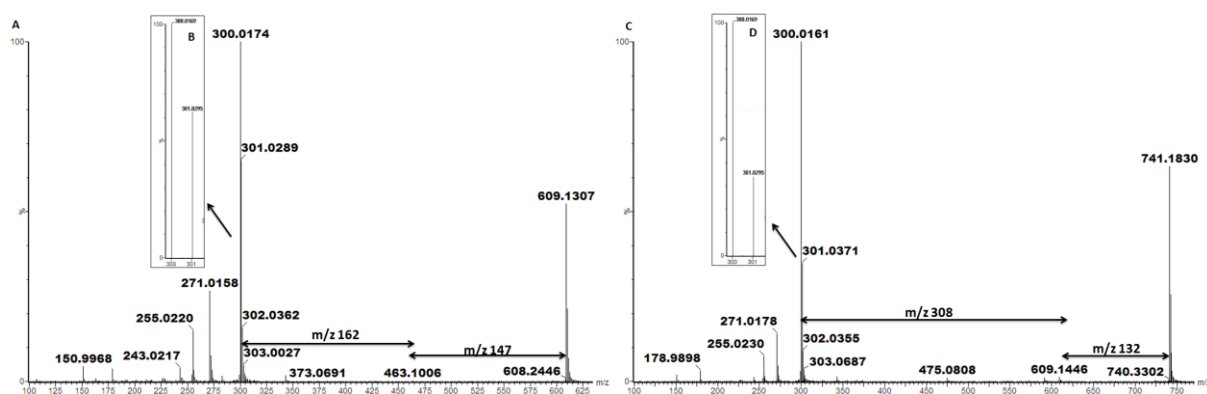


*Figure S2.21: Negative ion mode MS/MS spectrum of (A) rutin (m/z = 609.141) at Rt = 16.66 min with (B) an enlarged image of (A) [Y₀-H]⁻: $\overline{Y_0}$ ratio. Negative ion mode MS/MS spectrum of (C) quercetin-3-O-deoxyhexose-O hexose-O-pentose (m/z = 741.188) at Rt = 15.59 min with (D) an enlarged image of (C) [Y₀-H]⁻: $\overline{Y_0}$ ratio.*

The MS/MS spectrum of the precursor ion $m/z$ = 609.141 at Rt = 16.66 min (**Figure S2.21A**) shows the presence of a base peak at $m/z$ = 300.017. A weak ion peak is seen at $m/z$ = 463.101 corresponding to 147 Da consistent with the loss of a rhamnose moiety and the subsequent loss of 162 Da consistent with a glucose moiety. The fragmentation pattern seen in the MS/MS of this compound is consistent with that of quercetin-

glucose-rhamnose. **Figure S2.21** shows a zoomed in image of the ratio of $m/z$ = 300.017 to $m/z$ = 301.030 (designated $[Y_0\text{-}H]^-$ and $\overline{Y_0}$ respectively). By studying the ratio of $m/z$ = 300 to $m/z$ = 301 in the MS/MS spectrum of a flavonol-*O*-glycoside the position of their mono-*O*-glycosylation, their di-*O*-glycosylation or their mono-*O*-diglycosylation may be inferred.. According to literature when the $[Y_0\text{-}H]^-$ ion is more intense than the $\overline{Y_0}$ ion it indicates that the flavonol is 3-*O*-glycosylated. Thus the compound with precursor ion $m/z$ = 609.141 was identified as quercetin-3-*O*-rutinoside or rutin.

The MS/MS spectrum of the precursor ion $m/z$ = 741.188 at Rt = 15.59 min (**Figure S2.21C**) shows the presence of a base peak at $m/z$ = 300.016. A weak ion peak is seen at $m/z$ = 609.141, 741-609 = 132 Da corresponding to the loss of a pentose molecule and the subsequent loss of 308 Da consistent with the loss of a deoxyhexose molecule (146 Da) plus a hexose molecule (162 Da). The fragmentation pattern seen in the MS/MS of this compound is consistent with that of quercetin-3-*O*-deoxyhexose-*O*-hexose-*O*-pentose. **Figure S2.21D** shows an enlarged image of the ratio of $m/z$ = 300.017 to $m/z$ = 301.030 (designated $[Y_0\text{-}H]^-$ and $\overline{Y_0}$ respectively). The ratio of $m/z$ = 300 to $m/z$ = 301 indicates that the compound with precursor ion $m/z$ = 741.188 is quercetin-3-*O*-deoxyhexose-*O*-hexose-*O*-pentose.
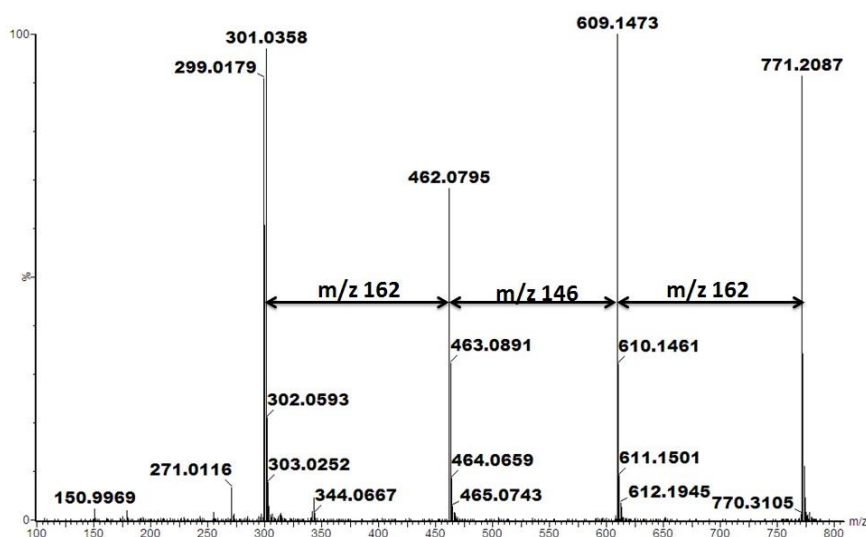


***Figure S2.22:*** *Negative ion mode MS/MS spectrum of quercetin-3-rutinoside-7-glycoside (m/z = 771.197) at Rt = 12.76 min.*

The MS/MS spectrum of the precursor ion $m/z$ = 771.197, seen in **Figure S2.22**, showed a base peak at $m/z$ = 609.147, corresponding to the loss of a glucose molecule of 162 Da. After the base peak the second most intense peak was seen to be at $m/z$ = 301, corresponding to the $\overline{Y_0}$ of quercetin. A less intense peak is seen at $m/z$ = 462, corresponding to the loss of 146 Da, a rhamnose molecule, after which another 162 Da, corresponding to a glucose molecule, is lost. The fact that the peak at $m/z$ = 462.080 is much less intense than those at $m/z$ = 609.147 and $m/z$ = 301.036 indicates that the first glucose molecule is isolated at one position while the subsequent glucose molecule is bonded to the rhamnose molecule at the other position. Unfortunately, it is difficult to know in which position, 3 or 7, the glycoside and the diglycoside are as these triglycosides do not

follow the normal $[Y_0\text{-H}]^-$ and $\overline{Y_0}$ ratio rules. Thus this compound was putatively identified as quercetin-3-rutinoside-7-glycoside.

**Figure S2.23** shows the differing levels of two different flavonoid glycosides, rutin (**Figure S2.23A**) and quercetin-3-*O*-deoxyhexose-*O*-hexose-*O*-pentose (**Figure S2.23B**), detected in each treatment group of each cultivar on day 8. The levels of rutin decreased in the **WF** treated groups of each cultivar relative to the controls. In the **S** cultivar, the levels of rutin decreased in the **WF** and the **WF+Vir** treated groups relative to the **S** control.
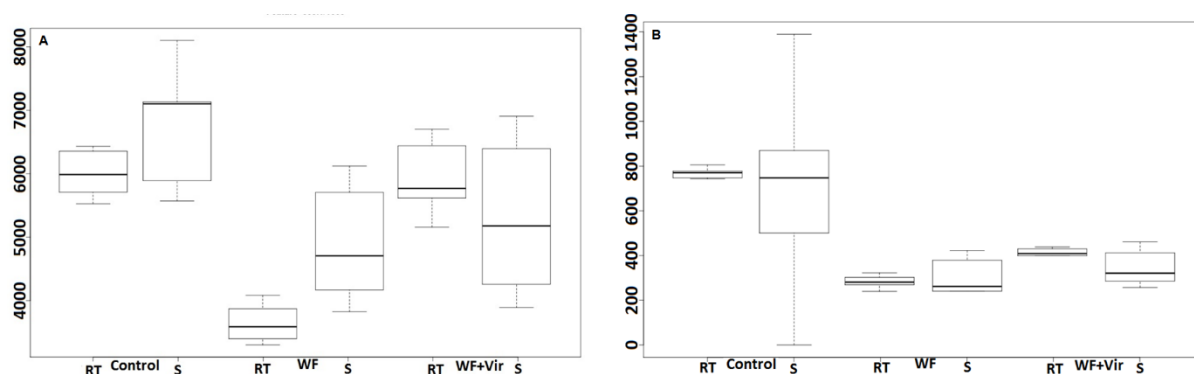


***Figure S2.23:*** *Box-and-whiskers plots showing the relative concentrations of (A) rutin (Rt = 16.66 min) and (B) quercetin-3-O-deoxyhexose-O-hexose-O-pentose acid (Rt = 15.59 min) in plants of different treatment groups and cultivars on day 8.*

## References

Clifford, M.N., Johnston, K.L., Knight, S., Kuhnert, N., Hierarchical scheme for LC-MS[n] identification of chlorogenic acids. *J. Agric. Food Chem.* **2003,** *51*, 2900–2911.

Clifford, M.N., Knight, S., Kuhnert, N., Discriminating between the six isomers of dicaffeoylquinic acid by LC-MS[n]. *J. Agric. Food Chem.* **2005**, *53*, 3821–3832.

Clifford, M.N., Kirkpatrick, J., Kuhnert, N., Roozendaal, H., Salgado, P.R., LC-MS[n] analysis of the *cis* isomers of chlorogenic acid. *Food Chem.* **2008**, *106*, 379–385.

López-Gresa, M.P., Lisón, P., Kim, H.K., Choi, Y.H., Verpoorte, R., Rodrigo, I., Conejero, V., Bellés, J.M., Metabolic fingerprinting of Tomato mosaic virus infected *Solanum lycopersicum*. J. Plant Physiol. **2012,** *169,* 1586-1596.

Ncube E, Mhlongo M, Piater L, Steenkamp P, Dubery IA, Madala N., Analyses of chlorogenic acids and related cinnamic acid derivatives from *Nicotiana tabacum* tissues with the aid of UPLCqTOF-MS/MS based on the in-source collision-induced dissociation method. *Chem. Cent. J.* **2014,** *8,*(1):66. doi: 10.1186/s13065-014-0066-z1–10.

Roldan, M.V.G., Engel, B., de Vos, R.C.H., Vereijken, P., Astola, L., Groenenboom, M., van de Geest, H., Bovy, A.G., Molenaar, J., van Eeuwijk, F.A., Hall, R.D., Metabolomics reveals organ-specific metabolic rearrangements during early tomato seedling development. *Metabolomics* **2014**, *10,* 958–974.